AIP | Review of Scientific Instruments

Maximizing the quantum efficiency of microchannel plate detectors: The collection of photoelectrons from the interchannel web using an electric field

Richard Cordia Taylor, Michael C. Hettrick, and Roger F. Malina

Citation: Review of Scientific Instruments **54**, 171 (1983); doi: 10.1063/1.1137365
View online: http://dx.doi.org/10.1063/1.1137365
View Table of Contents: http://scitation.aip.org/content/aip/journal/rsi/54/2?ver=pdfcov
Published by the AIP Publishing

Maximizing the quantum efficiency of microchannel plate detectors: The collection of photoelectrons from the interchannel web using an electric field

Richard Cordia Taylor, Michael C. Hettrick, and Roger F. Malina

Space Sciences Laboratory, University of California, Berkeley, California 94720

(Received 5 August 1982; accepted for publication 5 October 1982)

We report dependence of the extreme ultraviolet quantum efficiency (QE) of a microchannel plate (MCP) detector upon the electric field strength above its input face. Using an uncoated plate, we measured increases up to 80% as the field was raised from 0 V/μ to between 0.01 and 0.1 V/μ. Further increases in electric field resulted in a monotonic decrease in QE. Detector spatial resolution was found to degrade for these small field values but could be recovered, while maintaining most of the QE increase, by operating with fields in excess of 0.3 V/μ. Other detector parameters such as modal gain and output charge pulse-height distribution were not significantly affected by the applied electric field. We explain the QE and resolution variations in terms of photoelectrons ejected from the interchannel web and subsequently returned to the input face of the MCP by the applied electric field. We present a model and a computer simulation which quantitatively reproduce our experimental results. Applying our model to MCPs coated with photocathode materials, we conclude that the maximum QE is obtained by optimizing the combined contributions from the web area and open area of the MCP, rather than by maximizing the open area alone. In this case, most of the QE can arise from the interchannel web rather than from the directly illuminated channels.

PACS numbers: 07.62. + s, 29.40.Mc

INTRODUCTION

During the last decade, microchannel plate (MCP)[1] detectors have been widely used in x-ray,[2] extreme ultraviolet (EUV),[3,4] and ultraviolet[5] astronomy. High quantum efficiency, low background, and two-dimensional imaging capabilities make the MCP a suitable detector for a sky survey instrument. The Extreme Ultraviolet Explorer[6] satellite, to be launched in 1987, will use MCP detectors; and it was in the course of the instrument development for this program that the results described in this paper were obtained.

Although MCP detectors have good quantum efficiency, one feature of their construction inherently limits their efficiency: the walls of the individual channels which make up the channel plates are of finite thickness and thus form an interchannel web. Under normal circumstances, this web does not contribute to the detector's quantum efficiency. To overcome this limitation, schemes to decrease the area of the web have been tried, such as using square channels or funneled channels.[7] Research by Panitz and Foesch,[8] however, suggested that these complex manufacturing procedures might be unnecessary. They demonstrated that when an MCP was bombarded with ions, electrons were ejected from the electrode material coating the web. With a small electric field applied between the input face of the MCP and a grid above the face, these electrons were returned to the MCP surface where they were detected. Subsequent experiments used a similar principle to enhance the QE of MCPs to incident photons.[7,9] These results encouraged us to perform a detailed study of such enhanced quantum efficiencies, using extreme UV wavelengths.

I. EXPERIMENTAL ARRANGEMENT

A schematic of the instrument arrangement is given in Fig. 1. The MCPs were manufactured by Galileo Electro-Optics and had hexagonally packed round channels with a diameter of 25 μ, a channel separation of 31 μ and a bias angle of 8°. The open area of the MCPs was, therefore, 58%; the overall diameter was 25 mm. The channel length to diameter ratio was 40 : 1. The electrode material on the MCPs was chromium and extended one channel diameter into each channel. To achieve high gain, the channel plates were run in a tandem configuration with bias resistors setting voltages across each plate, between the plates,[10] and between the back plate and the anode. These bias resistors were chosen to operate the detector with a peaked pulse-height distribution with a resolution, defined as the FWHM of the distribution, between 120% and 185%. The peak of the distribution (the modal gain) was between 2.8×10^6 and 4.0×10^6 for the angle of incidence and wavelengths of the radiation used in the experiment. Electrons emerging from the rear MCP were proximity focused onto a two-dimensional resistive anode based on the geometry developed by Gear,[11] and Lampton and Carlson.[12] This type of detector arrangement, a RANICON, has been discussed in the literature.[13] The electronics' discriminator was set to ignore all pulses less than 0.5×10^6 gain. The anode was kept at ground

 0034-6748/83/020171-06$01.30

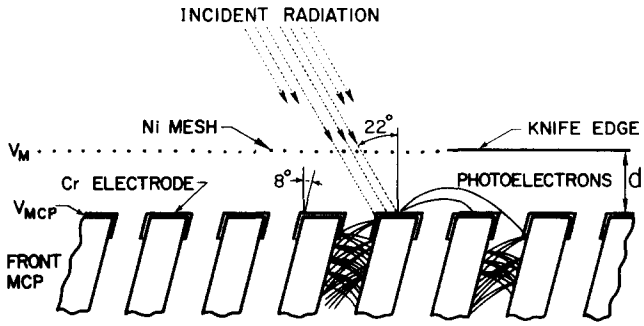

FIG. 1. Schematic of instrument arrangement. The electric field between the mesh and the channel plate is $E = (V_{MCP} - V_M)/d$.

while the input face of the front MCP was operated at −2500 V.

The front MCP was illuminated with a collimated beam of monochromatic EUV radiation. Emission lines from hydrogen and helium at 1216, 584, and 304 Å were generated by a hollow cathode source.[14] An aluminum III line at 170 Å was produced in a Penning discharge lamp.[15] Wavelengths were selected using a 2-m McPherson monochromator. The illuminating beam was then collimated by a pinhole to produce a spot approximately 6 mm in diameter on the input surface of the detector. The beam divergence was 0.1°. The light was incident at 30° to the direction of the channels of the front plate, or equivalently, at 22° to the normal of the detector. Typical count rates were 10^3–10^4 c/s, well below those at which significant MCP gain sag occurs.[16]

The input surface of the front channel plate of the RANICON was preceded by a nickel mesh as shown in Fig. 1. The spacing of the mesh wires was 1270 μ and the width of the wires was 127 μ. The mesh was 28 μ thick. For the 22° incidence angle of the radiation, the attenuation was 20%. The mesh was mounted 1800 μ from the input face of the channel plate; variations from planar field equipotentials are calculated to be less than 0.1% in the region from 30 to 530 μ above the MCP.

Absolute quantum efficiency measurements were obtained at 304, 584, and 1216 Å by calibrating against a

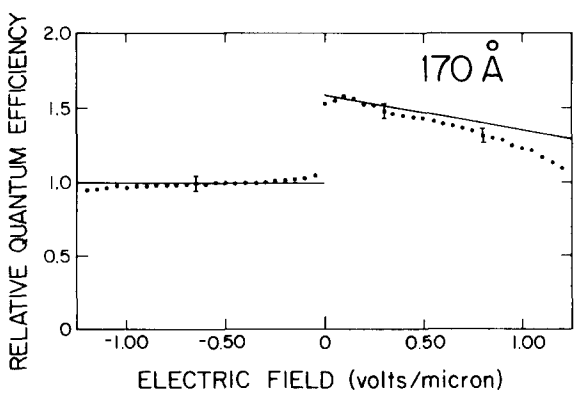

FIG. 2. Relative quantum efficiency (QE) at 170 Å, plotted vs the electric field above the input surface of the front MCP. Typical relative errors are indicated. Computer simulation fits are shown as solid lines. A relative QE of unity corresponds to an absolute QE in the range 0.006–0.06.

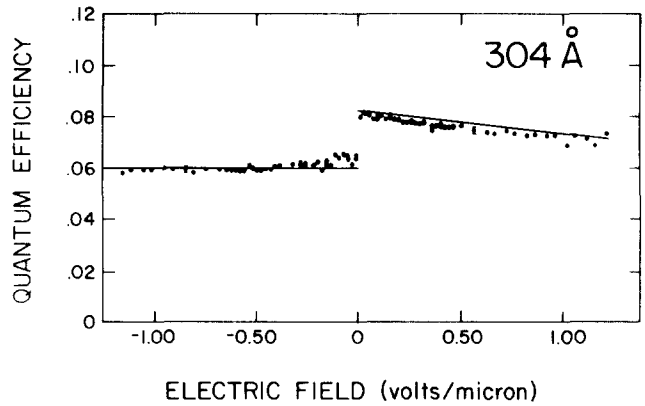

FIG. 3. Absolute quantum efficiency at 304 Å, plotted vs the electric field above the input surface of the front MCP. Typical relative errors are indicated. Computer simulation fits are shown as solid lines.

secondary standard channeltron[17] which had been calibrated against an NBS (National Bureau of Standards) diode. The absolute calibration accuracy is estimated at ±15%. Relative measurement errors varied from ±2% to ±4%. The data collected at 170 Å have larger errors than at the other wavelengths because of a much poorer signal-to-noise ratio at this wavelength and the greater variability of the Penning source intensity. Also, due to a large uncertainty in the absolute calibration at 170 Å, we report only relative QE values for this wavelength. A relative QE of unity corresponds to an absolute QE in the range 0.006–0.06.

Detector spatial resolution was measured by illuminating a knife edge preceding the front MCP and measuring the one-dimensional spatial profile in the unilluminated portion of the channel plate. The pulse-height distribution resolutions and modal gains were measured on a Hewlett–Packard pulse-height analyzer. The experiment was conducted in a vacuum below 4×10^{-6} Torr.

II. QUANTUM EFFICIENCY

We show in Figs. 2–5 the variation of detector quantum efficiency as a function of electric field. The field vector points from the input face of the MCP to the nickel mesh, for positive electric field values. The discrete points represent the experimental results for wavelengths of 170,

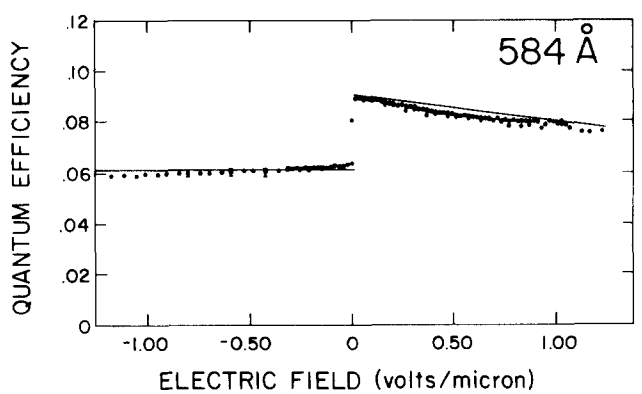

FIG. 4. Absolute quantum efficiency at 584 Å, plotted vs the electric field above the input surface of the front MCP. Typical relative errors are indicated. Computer simulation fits are shown as solid lines.

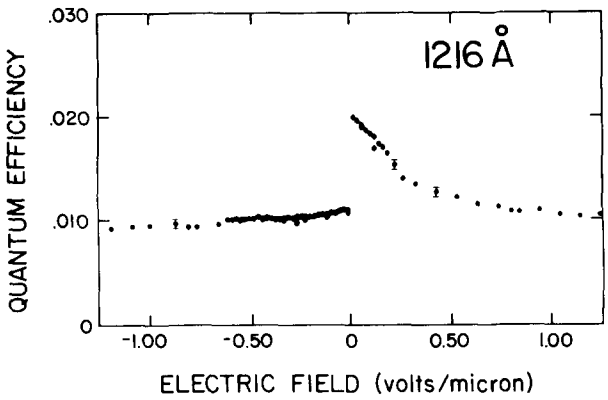

FIG. 5. Absolute quantum efficiency at 1216 Å, plotted vs the electric field above the input surface of the front MCP. Typical relative errors are indicated.

304, 584, and 1216 Å. Relative measurement errors are indicated in each figure. These quantum efficiencies include the 20% attenuation of the nickel mesh. The efficiency of the MCP alone is, therefore, 25% higher than shown. In the EUV, a thin-film filter commonly precedes the MCP. In this case, the electric field potential can be applied directly to the supporting mesh or a metallic filter, thereby introducing no additional attenuation.

As shown in Figs. 2–5, the results are qualitatively similar at all wavelengths. Between -1.25 and 0 V/μ, the QE increases monotonically by 7%, 13%, 8%, and 20% at 170, 304, 584, and 1216 Å, respectively. As the field direction is reversed to very small positive values ($\sim$0.01 V/μ), there is a large increase of 57%, 26%, 40%, and 80% at 170, 304, 584, and 1216 Å, respectively. As the field is increased further, the QE drops monotonically at all wavelengths. The drop in QE is most pronounced at 1216 Å, where 1 V/μ yields approximately the same value as was obtained with negative electric fields.

III. DETECTOR RESOLUTION, BACKGROUND, AND PULSE-HEIGHT DISTRIBUTION

We have studied the effect of an applied electric field on other MCP performance parameters, in order to determine the optimum operating conditions. Due to the ballistic trajectories of the photoelectrons ejected from the web, a point image on the web will be detected as a halo around the illuminated point. When the MCP is illuminated, the total image detected is a composite of directly illuminated channels and image halos. If the FWHM of the halo is large, image degradation will occur. In Fig. 6 we show the FWHM of the image halo as a function of the electric field at 304 Å. As shown, no halo is detected for negative electric fields. When the field becomes slightly positive, the halo FWHM abruptly increases coincident with the abrupt increase in QE shown in Fig. 3. As the field is increased further, the halo shrinks rapidly. For fields above 0.3 V/μ, the halo size is small enough that the intrinsic detector resolution of $\sim$100 μ precludes its measurement.

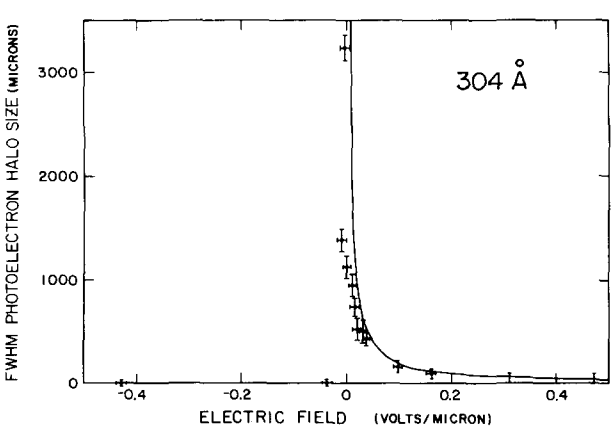

FIG. 6. FWHM photoelectron halo size dependence on electric field, at 304 Å. Computer simulation results are shown as a solid curve.

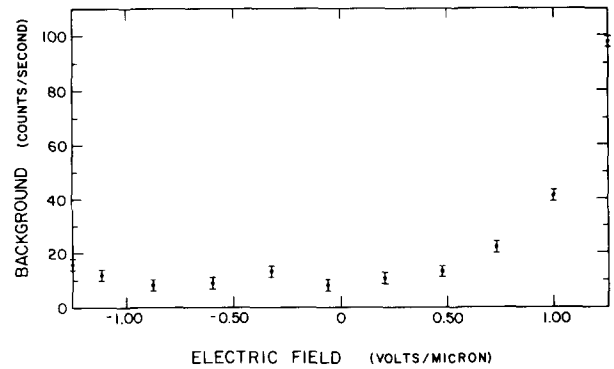

FIG. 7. Background count rate dependence on electric field.

In Fig. 7 we show the detector background count rate as a function of the electric field. As can be seen, there was no effect on the detector background until field values larger than 0.5 V/μ were reached. The field value of 0.5 V/μ corresponded to a grid voltage of -3400 V. As the field was increased further, the count rate was found to continue increasing, and became highly erratic. It is probable that this increase in background was due to field emission from the grid. Because of this, grid designs must minimize the number of sharp edges on high voltage surfaces.

The gain and pulse-height distribution from the MCP was also studied as a function of the electric field value. We found that the modal gain varied by less than 5% over all field values at each wavelength studied. The FWHM of the pulse-height distribution was found to change by less than 10%. We measured the pulse-height distribution (PHD) of the additional counts detected with the positive electric field, by subtracting a PHD collected with a negative field from a PHD collected with a positive field. The PHD for the interchannel events had a modal gain and pulse-height distribution FWHM identical to the channel events, to within 3%.

Combining our findings for spatial resolution, detector background, and pulse-height distribution, we find that at 304 Å it is best to operate with an applied electric field of between 0.3 and 0.5 V/μ. In this field range, none of the detector performance parameters are degraded, and the quantum efficiency increase is still large.

IV. THEORETICAL ANALYSIS

The QE variation due to the applied electric field can be understood in terms of the behavior of photoelectrons emitted in the channel throat and from the interchannel web. By varying the field near the input face of front MCP, the trajectories of these electrons will be influenced and the detector quantum efficiency altered.

As can be seen in Figs. 2–5, there is a small increase from 5% to 20% in the quantum efficiency as the field is raised from -1.25 to 0 V/μ at all of the wavelengths. For negative fields, there is a Schottky lowering of the potential barrier of the electrode material coating the web. This reduction is $\Delta\phi = (-eE/4\pi\epsilon_0)^{1/2}$ (= 0.042 V for $E = -1.25$ V/μ), and results in an enhancement of the photoelectric yield of the electrode material.[18] Due to the direction of the field, however, these additional photoelectrons will be collected by the mesh, and hence will not contribute to the quantum efficiency of the detector. The small increase from -1.25 to 0 V/μ is most likely due to field fringing at the throat of each channel. For grid voltages corresponding to negative field values, the zero-potential field surface intrudes into the channel throat. Hence, some of the photoelectrons ejected at the throat of the channel will be drawn out of the channel to the grid. As the field is increased, the zero-potential surface moves out of the channel throat, and more photoelectrons from the throat are counted.

As soon as the electric field direction between the input face of the MCP and the mesh becomes positive, all of the photoelectrons having insufficient energy to traverse this gap will return to the input face. The general features of this process are expressed in the following formula for the quantum efficiency:

$$\mathrm{QE} = \mathrm{QE}_{CH} \times (1 - W) + W(1 - W)yD_e, \quad 0 \leqslant W \leqslant 1, \tag{1}$$

where QE_{CH} is the quantum efficiency of the channels at the wavelength and angle of incidence in question, W is the fraction of detector area occupied by the interchannel web, y is the photoelectric yield of the web material at the relevant wavelength and angle of incidence, and D_e is the electron detection efficiency of the channels. Higher-order terms exist for secondaries produced from the photoelectrons that hit the web rather than the channels, and for photoelectrons that elastically collide with the web and then land in the channels. The complete form of Eq. (1) is thus

$$\mathrm{QE} = (1 - W)\left(\mathrm{QE}_{CH} + D_e \sum_{n=1}^{\infty} W^n \prod_{j=1}^{n} q_j\right), \tag{2}$$

where $q_1 = y$. The higher-order terms of Eq. (2) that are neglected in Eq. (1) can be shown to be bounded as follows:

$$\text{higher-order terms} = D_e(1 - W) \sum_{n=2}^{\infty} W^n \prod_{j=1}^{n} q_j \leqslant W(1 - W)yD_e\left(\frac{W\|q_j\|}{1 - W\|q_j\|}\right), \tag{3}$$

where $\|q_j\| = \max(q_j)$ and $W\|q_j\| < 1$. Since the electric field is conservative, photoelectrons will leave and hit the web with the same energy distribution. For these low-energy photoelectrons (most below 10 eV), the secondary-emission coefficients[19] q_j are between 10% and 55%. Taking $\|q_j\| = 55\%$, Eq. (3) predicts that the sum of the terms for $n \geqslant 2$ will contribute less than 30% of the $n = 1$ term. For our purposes, Eq. (1) is, therefore, a good approximation of Eq. (2).

Equations (1) and (2) also assume that the photoelectron initial and terminal locations are totally random on the input face of the MCP. This assumption is not completely valid. This discrepancy will be discussed below. Nonetheless, Eq. (1) accurately predicts the increase in quantum efficiency that we observed. For example, at 584 Å, the term $(1 - W)\mathrm{QE}_{CH} = 6.2\%$ as determined from our data. W is about 42% as we have determined from measurements of photomicrographs of the surface of Galileo channel plates. The photoelectric yield at 584 Å for most metals[20] is $\sim$10%, and the electron detection probability[21,22] is $\sim$90%, for electron energies less than 100 eV. With these values, a maximum quantum efficiency of 8.4% is calculated, which agrees well with our experimental result of 9%. Similar calculations for 304 and 1216 Å yield optimum quantum efficiency values of 7.8% and 1.8%, respectively, compared to our measured values of 8.5% and 2%. This agreement is good and is within the $\pm$15% error in absolute QE.

Equations (1) and (2) do not include the effects of the photoelectron trajectories. To include these, we rewrite Eq. (1) as

$$\mathrm{QE} = \mathrm{QE}_{CH} \times (1 - W) + yD_e \times F[E, \varphi(U), N(\theta), G, d], \tag{4}$$

where F is a function of the electric field, E, the photoelectron energy distribution, $\varphi(U)$, the photoelectron angular distribution, $N(\theta)$, the separation between the mesh and the MCP, d, and G a geometric description of the arrangement, size, and shape of the microchannels that perforate the input surface of the channel plate. To obtain Eq. (1), we ignored the dynamic functional dependences of $F[E, \varphi(U), N(\theta), G, d]$ and approximated

$$F[E, \varphi(U), N(\theta), G, d] = W(1 - W). \tag{5}$$

V. SIMULATION

We developed a computer simulation to generate the function $F[E, \varphi(U), N(\theta), G, d]$ accurately for the specific geometry of our experiment. In this simulation, a photoelectron contributes to $F[E, \varphi(U), N(\theta), G, d]$ only if it is emitted from the interchannel web, and after following a trajectory determined by its energy, angle of ejection, and by the electric field, enters a microchannel. We assume that the electric field E is constant between the mesh and the front of the MCP. This is a good assumption for the electric field in the region from one channel spacing above the MCP to one mesh spacing below the mesh. The distance r traveled by a photoelectron of energy U emitted

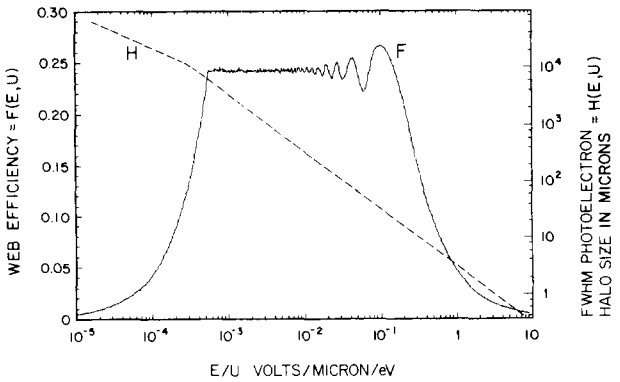

FIG. 8. Results of computer simulation for monoenergetic photoelectrons ejected from the interchannel web. $F(E, U)$ is the geometric contribution of the web to the quantum efficiency. $H(E, U)$ is the FWHM photoelectron halo size. The ordinate E/U is the electric field divided by the energy of the ejected photoelectrons.

at an angle θ to the normal to the surface is given by its ballistic trajectory as

$$r = \frac{2U \sin 2\theta}{Ee}. \tag{6}$$

The probability that a photoelectron is emitted at an angle θ to the surface normal is approximately[23]

$$N(\theta) = \sin 2\theta. \tag{7}$$

In the simulation, photons are incident on a channel plate whose front surface has the same channel spacing and channel diameter as our experimental channel plates. A distance between the mesh and the MCP of $d = 1800$ μ was used. On the average, 58% of the incident photons enter the channels directly, and 42% of the photons impinge on the web at random locations. As an initial assumption, we considered monoenergetic photoelectrons ejected from the web at random angles weighted by the angular distribution of Eq. (7). 10^9 photoelectrons/mm^2 were ejected at each voltage to minimize statistical fluctuations.

In Fig. 8 we show the results for monoenergetic photoelectrons. The function $F(E, U)$ is plotted vs E/U(V/μ/eV). The web contribution to the channel plate quantum efficiency is

$$\text{web contribution} = yD_e \times F(E, U). \tag{8}$$

These results confirm the validity of our initial assumption in Eqs. (1) and (5). From 6×10^{-4} to 2×10^{-1} V/μ/eV, the mean value of $F(E, U)$ is equal to $W(1 - W) = 0.24$. From 10^{-4} to 5×10^{-4} V/μ/eV, the rate at which $F(E, U)$ rises is set by the plate-mesh separation of $d = 1800$ μ.

Also plotted in Fig. 8 is the FWHM of the image halo $H(E, U)$ formed by the detection of photoelectrons from the interchannel web, as a function of electric field. The size of the halo is found to relate to the shape of $F(E, U)$. From 10^{-2} to 2×10^{-1} V/μ/eV, there are discernible modulations in $F(E, U)$, caused by the lattice arrangement of microchannels on the input face of the MCP. These modulations become large when the halo size is a few microchannels wide. The halo size is found to decrease with increasing electric field. The web's contribution to the quantum efficiency $F(E, U)$ decreases only for a halo radius less than 15 μm, which is about one-half of the separation between the channels. The high voltage fall-off above 2×10^{-1} V/μ/eV is due to photoelectrons not reaching the nearest channel, and being returned to the web.

To make a quantitative comparison of our model with our measurements, it was necessary to convolve $F(E, U)$ with the photoelectric energy distribution, $\varphi(U)$, for the material coating the web. The web surface material is a mixture of chromium and the chromium oxides. Photoelectric energy distribution data was unavailable for this surface composition. Soft x-ray photoelectron energy distributions (PEDs) for a mixture of aluminum and aluminum oxide, however, have been published by Henke *et al.*[24,25] We assumed that Henke's data approximated the PEDs that could be measured for a mixture of chromium and its oxides in the extreme UV and soft x-ray regions. According to Henke, the PED is essentially unchanged between 1 and 124 Å. We, therefore, have used his Al PED for 44.7 Å to simulate our 170 Å data. Due to qualitative similarity of our 170, 304, and 584 Å results, this distribution was also used for these wavelengths. The result of the convolution of the aluminum distribution with $F(E, U)$ was used with Eq. (4) to produce the solid curves on Figs. 2–4 at 170, 304, and 584 Å. As can be seen, these curves adequately reproduce the experimental data to better than 10%.

To produce these curves, we first fit a horizontal line from -1.25 to 0 V/μ to the mean value of QE measured at each wavelength. This fit of $\text{QE}_{CH}(1 - W)$ was made because our model does not quantitatively describe the negative field detector behavior. The slope of the curve from 0 to 1.25 V/μ was determined from the normalized convolution

$$F[E, \varphi(U)_{\text{Al}}] = \frac{\left(\int_0^\infty F(E, U) \times \varphi(U)_{\text{Al}} dU\right)}{\left(\int_0^\infty \varphi(U)_{\text{Al}} dU\right)}. \tag{9}$$

$F[E, \varphi(U)_{\text{Al}}]$ exhibited none of the modulations that were evident on $F(E, U)$ in Fig. 8. $F[E, \varphi(U)_{\text{Al}}]$ rises smoothly from 0 at 0 V/μ to a plateau of 0.24 from $\sim 10^{-2}$ to $\sim 10^{-1}$ V/μ, and then smoothly falls. The maximum value of $\text{QE} = \text{QE}_{CH}(1 - W) + yD_e \times F[E, \varphi(U)_{\text{Al}}]$ was fit to the data. This second fit was done to eliminate any errors that might be made in estimating (from reported yields or absorption coefficients[25,26]) the quantum yield y and the electron detection efficiency D_e as well as to adjust for the absolute error in measured QE. Over the range of our data, $F[E, \varphi(U)_{\text{Al}}]$ is approximately a line. Although the fit of the model to the data is seen to be good, it will be slightly better if the peak increase is taken as an average of the data in the plateau region predicted by the model.

Our model was also used to simulate the FWHM halo size as a function of the applied electric field. The solid curve on Fig. 6 is the result of the convolution

$$H[E, \varphi(U)_{Al}] = \frac{\left(\int_0^\infty H(E, U) \times \varphi(U)_{Al} dU\right)}{\left(\int_0^\infty \varphi(U)_{Al} dU\right)}, \quad (10)$$

and is a measure of the photoelectron image halo FWHM. This convolution is found to agree satisfactorily with the data at 304 Å. However, the method used to infer FWHM halo sizes from knife-edge measurements is imprecise, resulting in values uncertain to within a factor 2.

No simulations were done at 1216 Å. The pronounced reduction in QE at high electric fields indicates that the photoelectron energy distribution at 1216 Å is of a lower mean energy than at the other wavelengths. Above ~1000 Å, most of the incident photons are reflected and thereby not available for generating photoelectrons. The image halo radius is inferred to be approximately one channel separation, when the field is only 0.2 V/μ.

The difference between Fig. 5 and Figs. 2–4 illustrates that there is a necessary tradeoff when running channel plates with a fixed electric field, if the detector is operated over a large range of wavelengths. Between 0.3 and 0.4 V/μ, the spatial resolution is regained for 170, 304, and 584 Å, but the QE increase at 1216 Å has dropped by 70%. Depending on the application, a compromise electric field value must be chosen. A possible advantage is the ability to suppress or spectrally separate the longer wavelengths, due to their smaller halo sizes.

VI. COATED CHANNEL PLATES

Figures 2–5 show that even with the applied electric field, the quantum efficiencies are less than 10%. We have found these results to be typical for uncoated channel plates.[27] An examination of Eq. (1) reveals two terms which can increase the quantum efficiency of the detector: QE_{CH}, the quantum efficiency of the individual microchannels, and y, the photoelectric yield of the material coating the interchannel web. If the front of the channel plate is coated with a material having a high photoelectric yield, the web can contribute more to the detector's QE than do the channels that are hit directly by the incident radiation. This conclusion is valid even if the substance coating the channel-plate surface penetrates into the channels, since the photoelectric yield of a substance is strongly dependent on both the angle of incidence and wavelength of the incident radiation, and yields can be higher for the webbing.

Unpublished measurements by Martin[28] have shown this hypothesis to be the case for a CsI coated MCP with UV light incident at a large angle to the channels. They observed that with incident radiation of 1730 Å, at 28° to the channels and 20° to the normal of the MCP, the web coated with CsI was responsible for 79% of the total QE of the detector. This was the case even though the channel efficiency was also increased by coating the channel throat with CsI to a depth of one channel diameter.

If in Eq. (1), the QE is maximized with respect to W, the fraction of area occupied by the web, we find:

$$W = \frac{1}{2}\left(1 - \frac{QE_{CH}}{yD_e}\right), \quad W \geq 0. \quad (11)$$

From the results obtained by Martin, a value of $QE_{CH}/yD_e = 0.11$ is obtained. For these conditions, the optimum web area calculated from Eq. (11) would be 44.5%, or an open area of 55.5%. Hence, if a CsI-coated detector were operated at 1730 Å with 20° incident radiation, funneling the channel entrances would not increase the detector's quantum efficiency, but rather would decrease the efficiency. It should be noted here that in the construction of Eq. (1) from which Eq. (11) was derived, secondary electrons produced on the web were ignored. This is not a valid assumption with coated plates, since materials with high photoelectric yields tend to have high secondary-emission coefficients also. Examination of Eq. (2), however, shows that our conclusion still holds. The higher-order terms of Eq. (2), resulting from secondaries produced on the web, will tend to increase further the web's contribution to the detector's quantum efficiency.

ACKNOWLEDGMENTS

For many helpful discussions and suggestions, we would like to thank C. Martin, D. R. Rogers, P. Jelinsky, Dr. C. Carlson, and Dr. M. Lampton of the University of California Space Sciences Laboratory, Chris Parks of Lawrence Berkeley Laboratory, Dr. G. L. Weissler of the University of Southern California, Dr. H. E. Hinteregger of the Air Force Cambridge Research Laboratory, and Dr. B. L. Henke of the University of Hawaii. We also thank Dr. Stuart Bowyer of the University of California Astronomy Department for support and advice. This research was funded by NASA grant NAS5-24445.

[1] J. L. Wiza, Nucl. Instrum. Methods **162,** 587 (1979).
[2] R. Giacconi *et al.*, Astrophys. J. **230,** 540 (1979).
[3] W. Cash, S. Bowyer, and M. Lampton, Astrophys. J. **221,** L87 (1978).
[4] R. F. Malina, S. Bowyer, and G. Basri, Astrophys. J. (accepted).
[5] G. F. Hartig, W. G. Fastie, and A. F. Davidsen, Appl. Opt. **19,** 729 (1980).
[6] S. Bowyer, R. Malina, M. Lampton, D. Finley, F. Paresce, and G. Penegor, SPIE J. **279,** 176 (1981).
[7] R. F. Malina, Ph.D. thesis, University of California, Berkeley, 1979.
[8] J. A. Panitz and J. A. Foesch, Rev. Sci. Instrum. **47,** 44 (1976).
[9] J. G. Timothy, Rev. Sci. Instrum. **52,** 1131 (1981).
[10] D. Rogers, and R. F. Malina, Rev. Sci. Instrum. **53,** 1438 (1982).
[11] C. W. Gear, Proceedings for the Skytop Conference on Computer Systems in Experimental Nuclear Physics, 1969 USAEC Conf-670301, p. 552.
[12] M. Lampton and C. W. Carlson, Rev. Sci. Instrum. **50,** 1093 (1979).
[13] M. Lampton and F. Paresce, Rev. Sci. Instrum. **45,** 1098 (1974).
[14] F. Paresce, S. Kumar, and C. S. Bowyer, Appl. Opt. **10,** 1904 (1971).
[15] D. Finley, S. Bowyer, F. Paresce, and R. Malina, Appl. Opt. **18,** 649 (1979).
[16] E. H. Eberhard, ITT Electro-Optical Products Division, Technical Note No. 127, August, 1980.
[17] J. E. Mack, F. Paresce, and S. Bowyer, Appl. Opt. **15,** 861 (1976).
[18] C. I. Coleman, Appl. Opt. **17,** 1789 (1978).
[19] A. J. Decker, Solid State Phys. **6,** 251 (1958).
[20] J. A. R. Samson, *Techniques of Vacuum Ultraviolet Spectroscopy* (Pied Publications, Lincoln, Nebraska, 1980), p. 224.
[21] Galileo Electro-Optics Corp., Technical Memorandum 600.
[22] C. W. Carlson (private communication).
[23] T. C. Fry and H. E. Ives, Phys. Rev. **32,** 44 (1928).
[24] B. L. Henke, J. A. Smith, and D. T. Atwood, J. Appl. Phys. **48,** 1852 (1977).
[25] B. L. Henke, J. P. Knauer, and K. Premaratne, J. Appl. Phys. **52,** 1509 (1981).
[26] B. L. Henke, SPIE J. **316,** 146 (1981).
[27] R. C. Taylor, D. Rogers, K. Coburn, and R. F. Malina (in preparation).
[28] C. Martin (private communication).